Supporting Information

Accelerating materials discovery using integrated deep machine learning approaches

Weiyi Xia[1], Ling Tang[2], Huaijun Sun[3], Chao Zhang[4], Kai-Ming Ho[5], Gayatri Viswanathan[1,6], Kirill Kovnir[1,6], Cai-Zhuang Wang[1,5*]

[1]Ames Laboratory, U.S. Department of Energy, Ames, IA 50011, United States

[2]Department of Applied Physics, College of Science, Zhejiang University of Technology, Hangzhou, 310023, China

[3]Jiyang College of Zhejiang Agriculture and Forestry University, Zhuji, 311800, China

[4]Department of Physics, Yantai University, Yantai 264005, China

[5]Department of Physics and Astronomy, Iowa State University, Ames, IA 50011, United States

[6]Department of Chemistry, Iowa State University, Ames, IA 50011, United States.

*Corresponding authors: wangcz@ameslab.gov

1. Artificial neural network machine learning interatomic potential for La-Si-P

Fig. S1 shows the developed ANN-ML potential wells reproduce the *ab initio* calculated formation energies for a wide range of La-Si-P ternary compounds, even many of these compounds that are not included in the training data set.

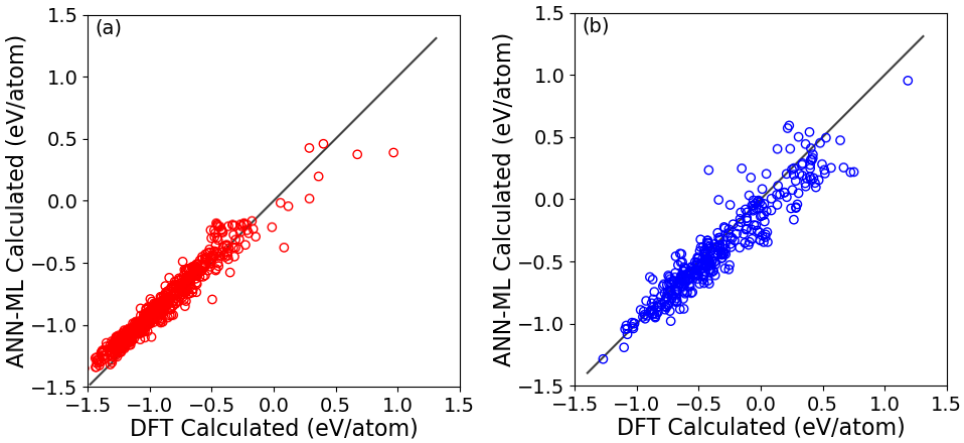

Fig. S1. The formation energies (E_f) of La-Si-P ternary compounds calculated by the ANN-ML interatomic potential are compared with the results calculated by DFT-PBE. (a) 806 La-rich La-Si-P ternary compounds from Ref (1), and (b) 353 P-rich La-Si-P ternary compounds from the present paper.

The La_2SiP_3 phase discovered in this paper was not included in the training data set. In order to demonstrate the reliability of the developed ANN-ML potential for MD simulations of the La_2SiP_3 phase at finite temperatures, 200 snapshots from AIMD simulations of La_2SiP_3 at 1200 K and 2500 K are randomly selected to validate the ANN-ML model for the interatomic force prediction in comparison with the *ab initio* calculation data. **Fig. S2** and **S3** show the comparisons between the forces obtained by *ab initio* simulations and the ANN-ML model prediction in La_2SiP_3 crystal at 1200K and La_2SiP_3 liquid at 2500K, respectively. The root mean square (RMS) force error for x, y, and z components is shown in the figures. **Fig. S4** shows a comparison of partial pair-correlation functions between AIMD and ANN-ML MD simulations for La_2SiP_3 liquid at T=2500K. It shows the ANN-ML MD simulation can well reproduce the atomic trajectory in AIMD simulation. These results indicate that the ANN-ML potential is reliable for MD simulation of La_2SiP_3 phase.

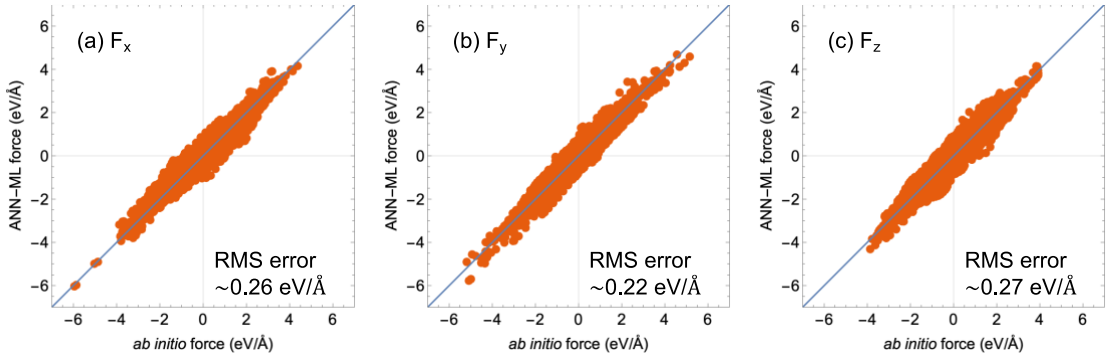

Fig. S2. Comparisons between the forces obtained by *ab initio* simulations and the ANN-ML model prediction in La_2SiP_3 crystal at 1200K.

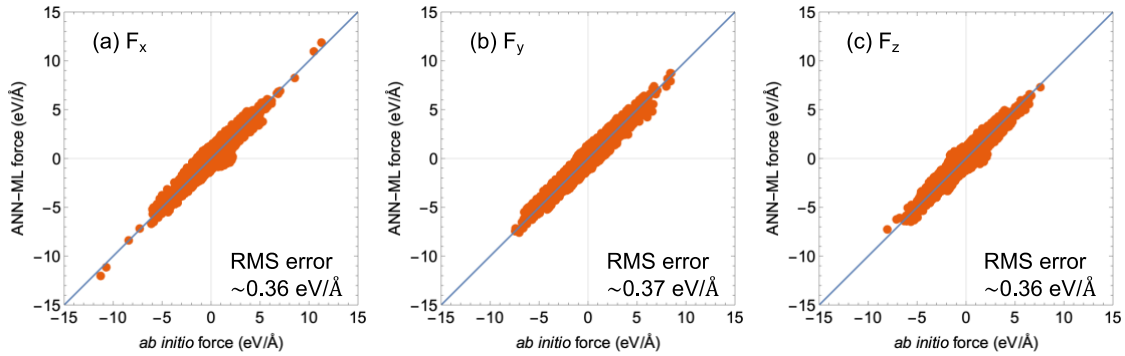

Fig. S3. Comparisons between the forces obtained by *ab initio* simulations and the ANN-ML model prediction in La_2SiP_3 liquid at 2500K.

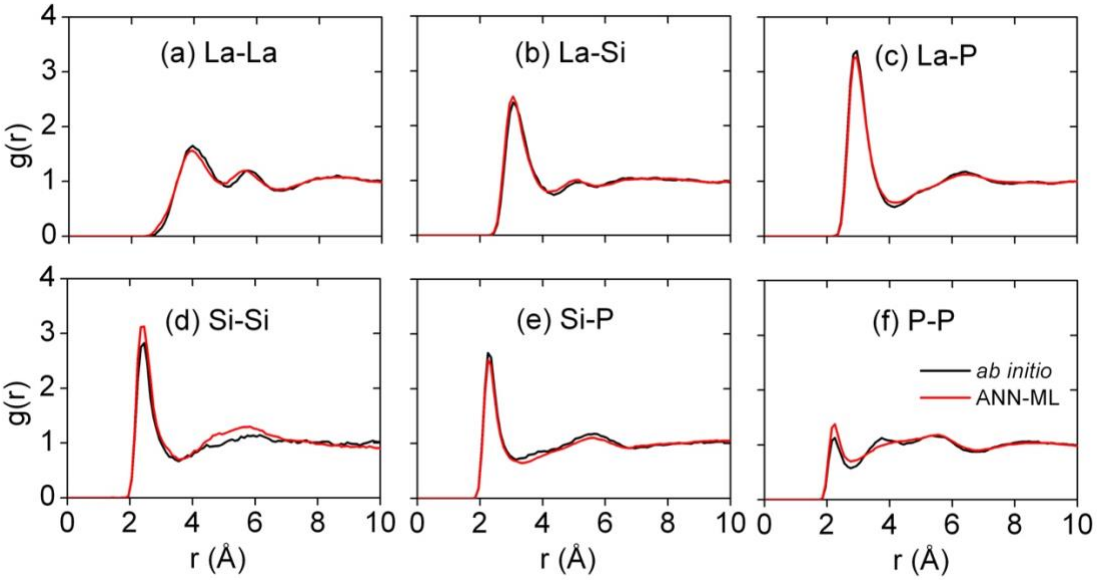

Fig. S4. Comparison of partial pair-correlation functions between AIMD and ANN-ML MD simulations for La_2SiP_3 liquid at T=2500K.

2. Electronic band structures of the two predicted La_2SiP_3 compounds

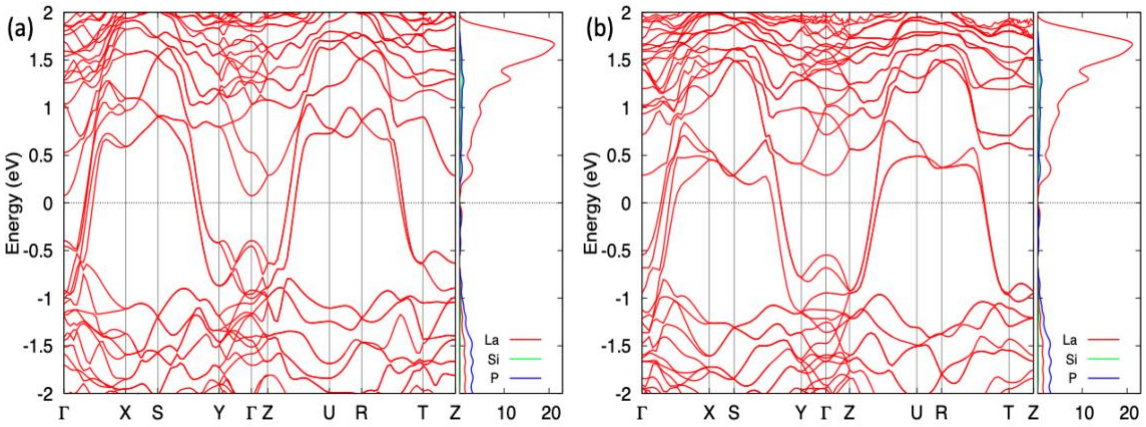

Fig. S5. The band structure and density of states of the two predicted La_2SiP_3 phases with the formation energies above convex hull (a) 1 meV/atom and (b) 33 meV/atom, respectively.

3. Gibbs free energies (at zero pressure) as a function of the temperature for known La-P and La-Si binaries and 5 ternary La-Si-P compounds

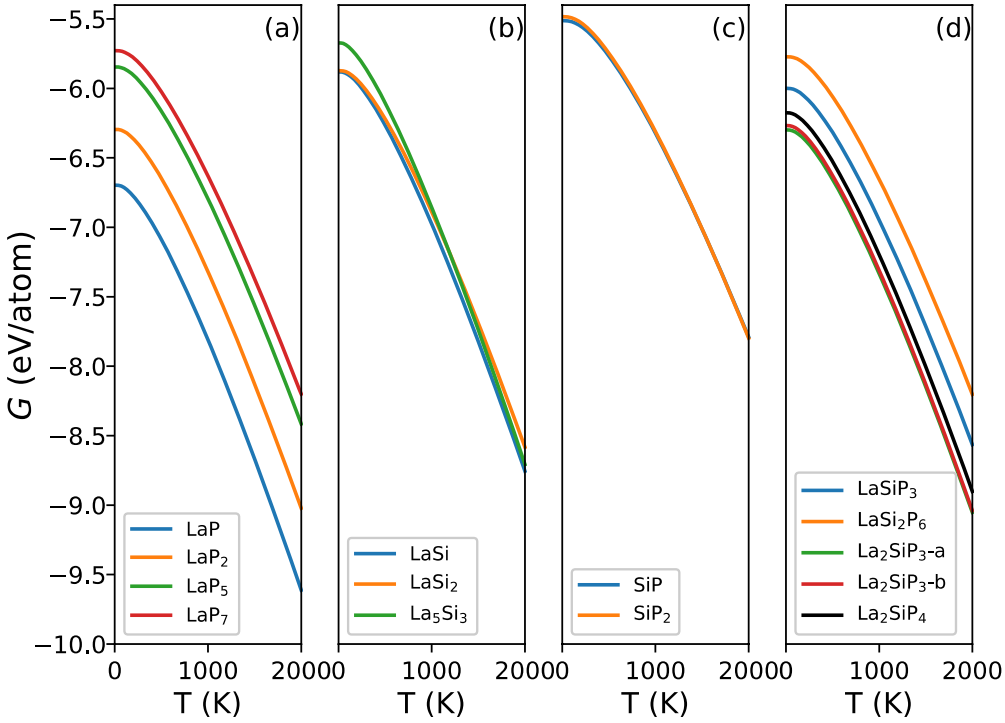

Fig. S6. Gibbs free energy (at p=0 kbar) as a function of temperature for (a) La-P binary

system, (b) La-Si binary system, (c) Si-P binary system, and (d) La-Si-P ternary system.

4. Electronic band structure of the predicted $BaLaSiP_3$ quaternary compound

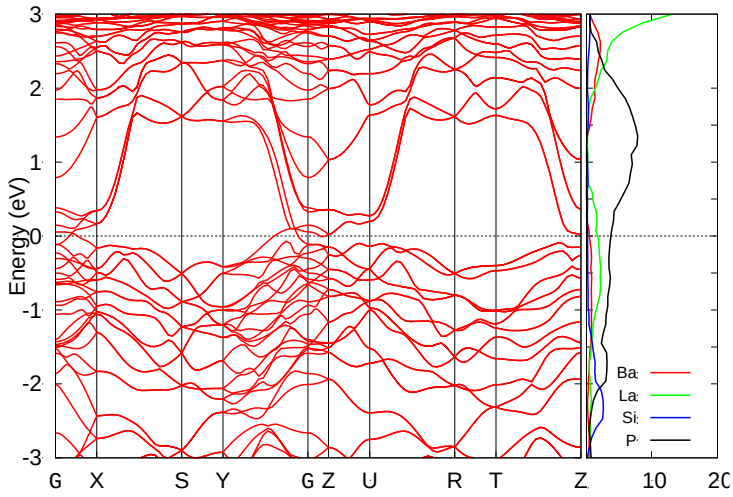

Fig. S7. The band structure and density of states of the predicted $BaLaSiP_3$ quaternary compound.

5. Gibbs free energies (at zero pressure) as a function of the temperature for relevant La-P, Ba-P binary, Ba-Si-P tenary, and Ba-La-Si-P quaternary compounds

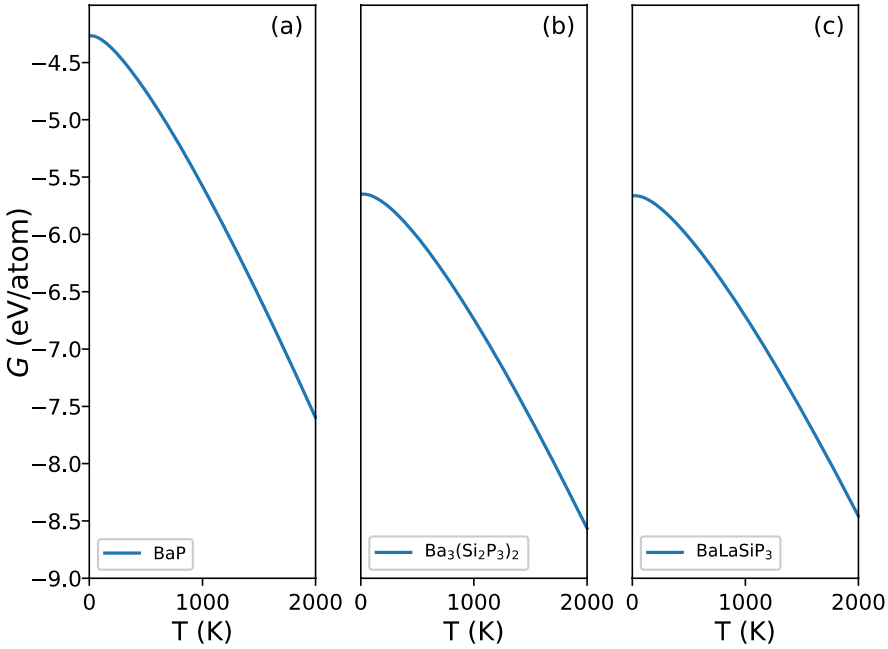

Fig. S8. Gibbs free energy (at p=0 kbar) as a function of temperature for (a) Ba-P binary system, (b) Ba-Si-P ternary system, and (c) Ba-La-Si-P quaternary system.

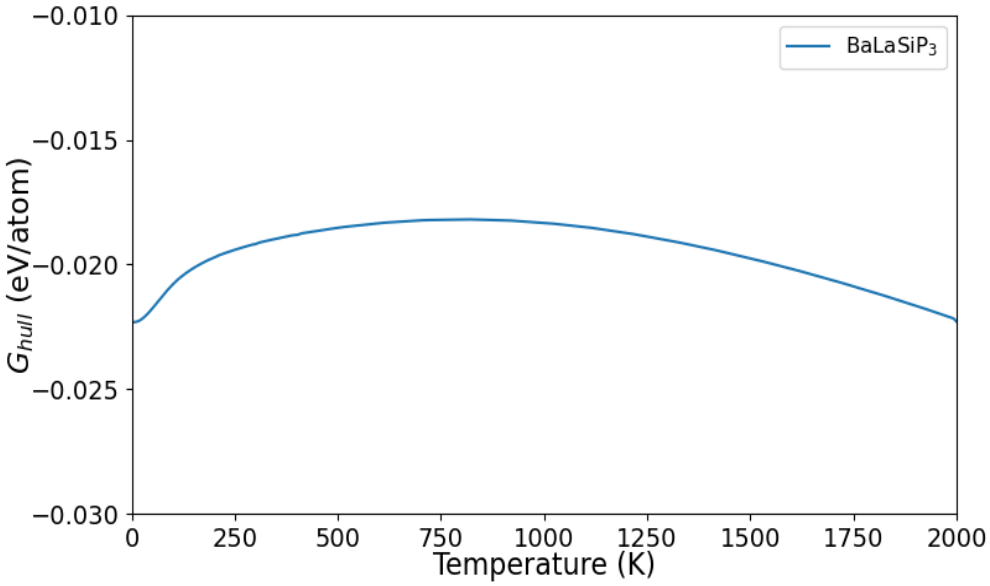

Fig. S9. Calculated G_{hull} as a function of temperature for the $BaLaSiP_3$ quaternary phase.

6. Structure information of the known and predicted low-energy binary and ternary compounds in La-Si-P system

Table S1. Structure database of the La-Si-P system, including existing phases, newly predicted stable phases and metastable phases. We list the space group, formula unit per cell, lattice parameters and the formation energies above the convex hull (E_d) of the elements (La,Si,P), binary, and all La-Si-P ternary compounds either existing or obtained from our ML-guided *ab initio* calculation prediction. The phases in bold are thermodynamically stable. The results are based on GGA calculations.

	Phases	Symmetry	f.u.	*a* (Å)	*b* (Å)	*c* (Å)	E_d (meV/atom)
Existing stable phases	**La**	*P*6$_3$/*mmc*	4	3.75	3.75	12.12	**0**
	Si	*Fd*-3*m*	2	5.44	5.44	5.44	**0**
	P	*P*-1	42	7.41	11.90	12.63	**0**
	La$_5$Si$_3$	*I*4/*mcm*	2	8.03	8.03	13.99	**0**
	LaSi	*Cmcm*	4	4.60	13.45	6.65	**0**
	LaSi$_2$	*I*4$_1$/*amd*	2	4.39	4.39	13.61	**0**
	LaP	*Fm*-3*m*	1	6.07	6.07	6.07	**0**
	LaP$_2$	*C*1*c*1	8	12.59	14.02	8.87	**0**
	LaP$_5$	*P*12$_1$/*m*	4	5.56	9.69	10.06	**0**
	LaP$_7$	*P*12$_1$/*c*	4	7.04	11.75	10.33	**0**
	SiP	*Cmc*2$_1$	12	3.52	20.52	14.41	**0**
	SiP$_2$	*Pbam*	8	3.44	10.19	14.98	**0**
	LaSiP$_3$	*Pna*2$_1$	8	8.08	8.08	23.43	**0**
	La(SiP$_3$)$_2$	*Cmc*2$_1$	8	10.20	10.20	10.20	**0**
ML+DFT predicted stable phase	**La$_2$SiP$_3$**	*Pnma*	4	8.14	4.19	16.12	**1**
Existing metastable phases	LaSiP$_3$	*Pbca*	8	5.78	5.98	25.54	87
	La$_2$SiP$_4$	*P*2$_1$/*c*	2	10.82	7.52	7.92	22
ML+DFT predicted metastable phases	LaSiP$_3$	*Pna*2$_1$	8	5.96	14.05	9.92	8
	La(SiP$_3$)$_2$	*Cmc*2$_1$	16	10.19	28.24	10.40	9
	La$_2$SiP$_3$	*Pnma*	4	4.14	11.32	11.73	33
	La$_5$(SiP$_4$)$_2$	*Cmce*	8	21.86	11.31	11.07	65
	La$_3$Si$_3$P$_7$	*P*6$_3$/*mc*	2	9.89	9.89	6.86	67
	La$_2$SiP$_3$	*Pnma*	4	4.05	11.23	12.55	71
	LaSi$_3$P$_5$	*R*32	12	13.12	13.12	16.01	78
	La$_3$Si$_8$P$_{14}$	*P*2$_1$/*c*	2	12.08	13.34	6.42	79
	LaSiP$_2$	*P*-1	6	7.06	8.98	10.93	80
	La$_2$SiP$_4$	*P*-1	4	5.92	9.46	12.01	86
	La$_3$Si$_{13}$P$_{21}$	*Cm*	4	24.71	14.29	9.08	91
	La$_5$(SiP$_2$)$_9$	*P*4/*ncc*	4	7.25	7.25	53.22	92
	La$_4$Si$_2$P$_7$	*P*2$_1$/*m*	2	8.67	6.43	11.38	94
	La$_2$SiP$_3$	*P*-1	2	6.15	7.00	7.70	94
	La$_5$Si$_4$P$_{10}$	*Fmm*2	4	11.55	13.10	10.95	98

Table S2. Crystallographic data of La$_2$SiP$_3$ (space group of *Pnma*), which has the formation energy above convex hull E_d = 1 meV/atom.

Phase	Lattice param.	Wyckoff site	Atom	x	y	z
La_2SiP_3	*a*=8.14 *b*=4.19 *c*=16.12 α=β=γ=90°	4c	La	0.75339	0.25	0.45491
		4c	La	0.58802	0.25	0.71027
		4c	Si	0.62554	0.25	0.13288
		4c	P	-0.00529	0.25	0.60344
		4c	P	0.87255	0.25	0.06783
		4c	P	0.67369	0.25	0.27158

Table S3. Crystallographic data of $BaLaSiP_3$ (space group of *Pnma*), which is energetically stable.

Phase	Lattice param.	Wyckoff site	Atom	x	y	z
$BaLaSiP_3$	*a*=8.67 *b*=4.06 *c*=17.27 α=β=γ=90°	4c	Ba	0.24446	0.75	0.45977
		4c	La	0.07878	0.75	0.71825
		4c	Si	0.14164	0.75	0.13288
		4c	P	0.00804	0.25	0.10885
		4c	P	0.12410	0.25	0.58805
		4c	P	0.17589	0.75	0.27054

References

(1) H. J. Sun, C. Zhang, W. Y. Xia, L. Tang, G. Akopov, R. H. Wang, K. M. Ho, K. Kovnir, and C. Z. Wang. Machine learning guided discovery of ternary compounds containing La, P and group IV elements. Inorganic Chem., 61:16699, 2022.